SAND2019-6428J

Explosion Hazards from Lithium-Ion Battery Vent Gas

Austin R. Baird[1,2]
Erik J. Archibald, P.E.[1]
Kevin C. Marr, Ph.D., P.E.[1]
Ofodike A. Ezekoye, Ph.D., P.E.[1]

[1]The University of Texas at Austin Department of Mechanical Engineering
[2]Sandia National Laboratories Building & Fire Safety Department

June 3, 2019

Abstract

Lithium-ion battery technology is rapidly being adopted in several high growth industries, including transportation and energy storage. Safety concerns, in particular, fire and explosion hazards, are threatening widespread adoption. In a thermal failure event, lithium-ion batteries can undergo thermal runaway, which can result in the release of flammable gases and pose fire and explosion hazards.; however, there is little available information characterizing the flammability properties of the gases released during a thermal. In this paper, analytical and modeling methods to estimate key characteristics, such as lower flammability limit, laminar flame speed, and maximum over-pressure are evaluated for use in quantifying the effect of cell chemistry, state-of-charge and other parameters on the overall hazard potential.

Highlights

- Review of flammable gas production by various lithium-ion cell chemistries
- Use of open source Cantera software to calculate vent gas flammability characteristics
- Estimation of lower flammability limit (LFL) including the effect of diluents
- Computation of vent gas flame speed for cells with different cathode chemistries and states of charge
- Quantification of maximum explosion pressure for cells with different cathode chemistries
- Summary of cell fire/explosion hazard by chemistry

Acknowledgement

This work is supported by the United State Department of Homeland Security under grant number EMW-2016-FP-00833 and Sandia National Laboratories Critical Skills Master's Program

Sandia National Laboratories is a multimission laboratory managed and operated by National Technology and Engineering Solutions of Sandia LLC, a wholly owned subsidiary of Honeywell International Inc. for the U.S. Department of Energy's National Nuclear Security Administration under contract DE-NA0003525. SAND No. 2019-#####

1 Introduction

Fire and explosions from thermal runaway of lithium-ion batteries have been observed in consumer products, e-mobility vehicles, electric vehicles, and energy storage applications. Several instances of thermal runaway have occurred for in consumer devices such as mobile phones, laptops, hoverboards, and e-cigarettes. Additionally, electrical vehicle incidents have resulted in larger fires. In 2017, an explosion of a train car in Houston, Texas was attributed to lithium-ion batteries being transported to a recycling facility. The explosion was so violent that windows broke on buildings up to 500 feet away [1, 2]. Large fire events have also occurred. In 2017, a containerized lithium-ion ESS burned at a utility plant near Brussels, Belgium. The ESS in Belgium was equipped with fire detection and suppression which failed to extinguish the fire [3]. In 2018 a cement plant in Jecheon, North Chungcheong Province experienced over $3 million in damage. This was the 15th reported ESS fire in Korea in 2018 [4]. In April 2019, a 2 MW ESS system at a solar facility in Surprise, AZ exploded resulting in 8 firefighters being injured [5]. It was reported that the explosion caused both chemical skin burns and chemical-inhalation burns [6]. This incident comes after a 2012 fire had already occurred in Surprise, Arizona [7], which lead to improved safety requirements at the time. Even with this hazard being known in Arizona, it is clear that additional safety analysis needs to be performed to prevent future occurrences and incidents.

Lithium-ion battery failures can result from a variety of sources including manufacturing defects, thermal abuse, electrical abuse and/or mechanical damage. In some instances, these failures within lithium-ion battery systems can lead to an exothermic reaction, causing the cell to undergo thermal runaway. In a thermal runaway event, a series of exothermic reactions increases the cell temperature, resulting in internal generation of gases. These gases build within the cell and can ultimately lead to rupture of the cell and release of the gases. The gas mixture generated and released is flammable, consisting of various mixtures of hydrogen, carbon-monoxide, carbon-dioxide and various hydrocarbons including methane and propane. Ignition of these gases result in fire and explosion scenarios that pose a significant risk to surrounding life and property.

Lithium-ion battery use is rapidly expanding for energy storage in residential, commercial, industrial and transportation markets. In these applications, batteries several orders of magnitude larger than those in consumer products are required. Lithium-ion battery energy storage systems (Li-BESS) designed for the residential and electric grid applications can be as large as tens of kilowatt-hours and megawatt-hours, respectively. In the design of these systems, engineers must balance performance, cost, size, weight and safety concerns. Achieving a high level of safety is especially important in applications in densely populated environments, such as indoor Li-BESS installations, where a thermal-runaway event is more likely to lead to high losses. While performance measures are generally well characterized for battery designers, safety aspects are less well-defined. Safety guidelines and requirements for lithium-ion batteries required for applications such as energy storage are slowly emerging in current and proposed codes and standards. For example, requirements for Li-BESS in buildings have been added to NFPA (National Fire Protection Association) 1 Chapter 52 [8]. Additionally, an ESS specific standard NFPA 855 [9], is currently under development. However, codes and standard specifically for lithium-ion battery systems are still evolving, and many of these codes and standards require performance-based analysis to ensure life safety.

Typically, fire and explosion risk is quantified by assessing both the probability and consequences of an event. Although the probability of an explosion is low, the consequences can be extremely high. Some explosion risk mitigation strategies include flammable gas exhaust, deflagration venting, inerting, suppression, hardening and increased standoff distance to personnel and assets. These strategies require characterization of three key gas properties: lower flammability limit of the gases, flame speed, and the maximum adiabatic overpressure.

In this work, models are presented that can be used to evaluate fire and explosion hazard for lithium-ion battery systems. Various lithium-ion battery cell chemistries, constructions, and states of charge are considered. Methods of estimating lower flammability limit, laminar flame speed and maximum overpressure of the gases released during thermal runaway are discussed. A model is also presented to use these metrics to predict the pressure time history of an explosion.

1.1 Battery Vent Gas Characterization

Several studies have characterized battery gases released during thermal runaway through experimental testing. These studies are summarized in Table 1. In many of these studies, lithium-ion cells are failed in an enclosed chamber, which allows for the test environment to be modified. The resulting gases are extracted

from the chamber and analyzed. In other studies, lithium-ion cells are failed under an exhaust hood. In these tests, the vent gas in the exhaust duct is extracted and analyzed. Measurements include vent gas composition, flammability limits and maximum pressure for battery cells of differing constructions and chemistries at varying states-of-charge (SOC). The cathode chemistries that are most typically analyzed are lithium-cobalt oxide (LCO), lithium-manganese-cobalt oxide (NMC), lithium-iron-phosphate (LFP) and lithium-nickel-cobalt-aluminum oxide (NCA).

Table 1: Summary of Cell Vent Gas Literature

Reference	Type of Cell	Cathode Chemistry	Electrolyte	Initial SOC (%)	Failure Environment	Failure Test
Kumai (1999) [10]	18650	LCO	PC:EMC: DEC:DMC	0%	Vacuum	Cycled/Overcharged/ Overdischarged at 25 C
Ohsaki (2005) [11]	Prismatic 633048	LCO	EC:EMC	OCH	N/P	Overcharged at 1 C Rate
Kong (2005) [12]	18650	LCO, LMO, LFP	EC:DEC	OCH	Ambient Conditions	Overcharged
Doughty (2005) [13]	18650	NCA	EC:PC:EMC & EC:EMC	100%	N/P	Thermal-Abuse (ARC)
Abraham (2006) [14]	18650	NCA	EC:EMC	100%	N/P	Thermal-Abuse (ARC)
Roth (2008) [15]	18650	NCA	EC:EMC	100%	Sealed Container	Thermal-Abuse (ARC)
Ribiere (2011) [16]	Pouch Cells	LMO	EC:DEC:DMC	0/50/100%	Air	Thermal-Abuse (Tewarson calorimeter)
Somandepalli (2014) [17]	Pouch Cells	LCO	ED:DEC	50/100/150%	Argon	Thermal Abuse (Combustion chamber)
Golubkov (2014) [18]	18650	LCO/NMC, NMC, LFP	DMC:EMC:EC & DMC:EMC:EC:PC	100%	Argon	Thermal Abuse (Reactor Chamber)
Larsson (2014) [19]	Battery Packs	LFP	N/P	0/50/100%	Air	Thermal Abuse (Fire Test Chamber)
Spinner (2015) [20]	18650	LCO	DMC:EC:PC	N/P	N/P	Thermal Abuse on Overcharged Cells(Fire Test Chamber)
Fu (2015) [21]	18650	LCO	N/P	0/50/65/ 70/100%	Air	Thermal-Abuse (Cone-calorimeter)
Yuan (2015) [22]	Prismatic	LFP	EC:DEC:EM	Varied from 100% to 190%	Air	Overcharged
Golubkov (2015) [23]	18650	NCA, LFP	EC:DMC:EMC:MPC & EC:DMC:EMC:PC	Varied from 0% to 143%	Inert Gas	Thermal Abuse
Sun (2016) [24]	18650	LCO, LMO, NMC, LFP	N/P	OCH	Air	Thermal Abuse on Overcharged Cells (Combustion Chamber)
Zheng (2016) [25]	Pouch Cells	LFP	EC:DMC:EMC	0%	N/P	Overdischarged (Glove Box)
FAA Study (2016) [26]	18650	LCO	N/P	0% thru 100%	Nitrogen 10 psia	Thermal-Abuse (Cone-calorimeter)
Lammer (2017) [27]	18650- (32A, 35E, MJ1)	NCA	N/P	100%	Inert Gas	Thermal Abuse
Larsson (2017) [28]	Pouch, Cylindrical	LCO, LFP, NCA-LATP	N/P	100%	Air	Thermal Abuse (Fire Test Chamber)
Fernandes (2018) [29]	Cylindrical, 26650	LFP	DMC:EMC: EC:PC	190%	Air Tight Polypropylene Enclosure	Overcharged (Explosion Proof Room)

Three types of failure tests have been used in the various studies that speciated the vent gas: Accelerating Rate Calorimetry (ARC), thermally abusing the cells with heaters or overcharging/discharging/cycling the cells. The failure tests used in each study is specified in Table 1 above. Parameters that were not provided by the study are denoted N/P. For tests that involved open flames or cone calorimetry, it is assumed that failure occurred in air. If a failure occurs in a non-inert environment, the reported vent gas composition will be slightly different due to some reactions taking place with the surrounding atmosphere. The vent gas composition from these tests is summarized in Figure 1 below.

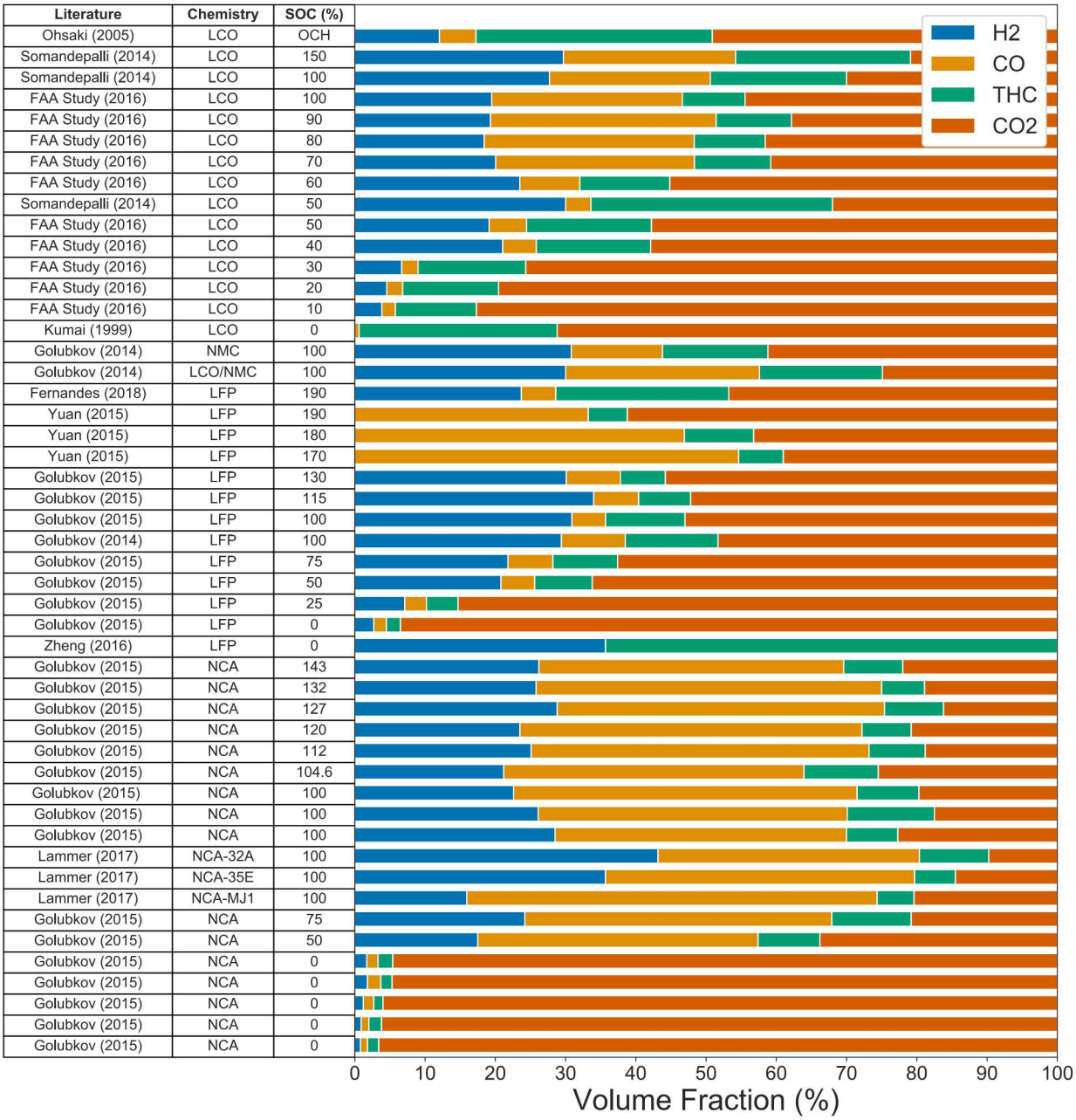

Figure 1: Battery Vent Gas Species Compositions from Literature

Figure 1 shows all the species composition from the reviewed literature by volume fraction. For hazard analysis, this review gives only the composition break down and not the total volume released. The species making up the vent gas is hydrogen, carbon-monoxide, hydrocarbons, and carbon-dioxide. It is clear that as the SOC increases, the fraction of hydrogen and carbon-monoxide increase while the carbon-dioxide decreases, Also, the total fraction of hydrocarbons remains relatively constant, anywhere from 10-15% for the NCA and LFP cells, and about 20-25% for the LCO cells. Since carbon-dioxide is an inert or non-flammable gas it actually helps reduce the hazard of the vent gas mixture. Yet with increasing SOC, the amount of carbon-dioxide in the vent gas decreases, which increases the overall hazard due to less inert gas by volume.

Further observations show a distinct change in the species composition of the vent gas once the SOC is at 40-50%, the total hydrogen production increases to about 20% for each chemistry above the 40-50% SOC. The LCO chemistry has data points from 0-30% SOC, and the flammable gases take up less than 25% of the volume production combined. Yet at 40% SOC, there is a sudden jump in the flammable gas production and a decrease in the carbon-dioxide per volume. The LFP cells have a similar trend at 25% SOC, as the total flammable gas

production is below 20% of the volume fraction. Yet at 50% SOC, the flammable gas production is above 30% by volume and increases further as the SOC increases. The NCA cell data only has data at 0% SOC or at 50% and higher SOC. Yet the trends for the LCO and LFP shows a significant reduction in overall hazard at a SOC below 40%.

Some additional observations were made for specific studies. In 2017, Lammer et al. [27] reported that 18650 cells from different manufacturers with the same cathode chemistry produce different vent gas compositions. This might be related to variation in cell manufacturing or the electrolyte species directly affecting the vent gas. The data from Yuan et al. [22] and Kumai et al. [10] were not used in the models because there was no hydrogen reported. In 2018, Fernandes et al. [29] conducted tests using the same cathode chemistry and SOC as Yuan, and hydrogen accounted for about 25% of the volume of the vent gas composition. Fernandes also brought up this variation when reviewing Yuan's work. Kumai specifically states that hydrogen was not measured or reported yet in similar studies it is measured and reported.

2 Vent Gas Hazard Metrics and Models

In explosion hazard analysis, lower flammability limit (LFL), laminar flame speed, and maximum overpressure are key metrics used to evaluate the overall hazard. The vast majority of previous studies do not directly measure or determine these parameters for battery vent gases. In the absence of experimental data, modeling tools can be used to evaluate the overall explosion hazard. Open-source chemical kinetics modeling tool (Cantera) and zero-order explosion models developed in-house are used to estimate LFL, flame speed, and max overpressure for the battery vent gas compositions measured in previous studies.

The primary modeling tool used for computing inputs for LFL prediction, laminar flame speed, and maximum pressure is Cantera [30]. Cantera is an open source chemical kinetics program that runs through Python, MATLAB, Fortran or C++. Cantera uses a Gibbs energy minimization for computing equilibrium products of combustion for various processes (e.g., constant pressure combustion, constant enthalpy combustion, etc.). The program also has a one-dimensional flame function that models freely-propagating premixed laminar flames. For the laminar flame analysis, the fuel species and air can be adjusted by altering the equivalence ratio and equilibrating the mixture for further characterization. Transport data and molecular properties for gas species used in Cantera come from GRI-Mech. Using GRI-Mech, chemical reactions can be modeled for natural gas flames [31]. Some of the different parameters in GRI-Mech include elementary chemical reaction rates, transport coefficients, molar heat capacity, entropy, and standard enthalpy. Due to the nature of the program and the overall goal, some of the species from the hydrocarbons measured by researchers in the literature review for the battery vent gas composition measured were not included in GRI-Mech. Taking this into account, some of the species were binned and the volume fraction of those species was added to propane. The binned species consist of hydrocarbons, C_xH_y, with a value for x of three or greater. With the larger molecular mass, propane is the most similar species to the ones not in Cantera. With most of the vent gas compositions obtained from available literature having less than 10% of the gas by volume being binned into propane, it will be shown that this binning does not have a large effect on the overall flame speed. A sensitivity study was performed by binning the volume fraction into propane compared to methane and the results are further discussed in section 2.2.

2.1 Lower Flammability Limit

The first metric to establish is estimating the range of lower flammability limit for the vent gas compositions. The LFL is important for fire and explosion analysis because it defines the volume fraction of fuel required to create the potential for a fire or explosion. Different codes, standards, and practices have specific requirements regarding LFL. This is the main motivation behind understanding and investigating LFL further. One example is NFPA 1 Ch. 52 which states that ventilation is required to keep the flammable gas concentration limited to 25% of LFL, otherwise, a ventilation rate of 1 CFM/ft^2 (5.1 L/sec/m^2) must be maintained or activated with gas detection.

Different methods to estimate the LFL for the battery vent gas compositions have been performed in the literature. Somandepalli et al. [17] determined LFL experimentally using a combustion vessel by measuring the fuel concentration at which the maximum overpressure was slightly greater than atmospheric pressure. An

FAA study [26] used Le Chatelier's mixing law [32] given in Equation 1, which gives LFL of the mixture based on the volume or mole fractions for fuel species.

$$\frac{1}{X_{\mathrm{L}}} = \sum_{i=1}^{fuels} \frac{X_{\mathrm{i}}}{X_{\mathrm{L_i}}} \tag{1}$$

Using Le Chatelier's law to compute the LFL of each cathode chemistry at 100% SOC gives various ranges based on the cathode chemistry: LCO varies between 6.5% to 7.5%, LFP varies between 8.3% to 8.7% and NCA varies between 6.2% to 9.8%. NCA cells have such a larger range for LFL due to the different failure test conditions for the datasets at 100% SOC.

There is some uncertainty with using Le Chatelier's law. Le Chatelier's law is mainly intended for only hydrocarbons and may not be appropriate for battery vent gas as it also contains hydrogen and carbon-monoxide as well as the inert diluent carbon-dioxide. Another method to determine LFL for an air-fuel- diluent mixture is to calculate the critical adiabatic flame temperature (CAFT). This method is appropriate for mixtures which contain inert diluents such as carbon-dioxide [33] as seen in Equation 2.

$$X_{\mathrm{L}}(T_{\mathrm{u}}) = \frac{\tilde{c}_{\mathrm{p,u}}(T_{CAFT} - T_{\mathrm{u}})}{\triangle h_{\mathrm{c}}} \tag{2}$$

In the standard CAFT method, the critical temperature for hydrocarbon mixtures is 1573K. This is inappropriate for mixtures containing hydrogen. Corrections for such mixtures are discussed later. The study by Zlochower et al. [34] shows the theoretical adiabatic flame temperature for hydrocarbons such as ethylene and methane range from 1390 to 1484 K at LFL. Hydrogen has a theoretical adiabatic flame temperature of approximately 734 K at LFL from Le et al. [35]. Other methods such as Beyler's Method to predict LFL and the method described by Ma et al. [36] also have a limitation in predicting LFL for gas mixtures involving hydrogen, hydrocarbons, and diluents.

Studies have been conducted to determine alternative ways to modify and apply Le Chatelier's law. A report prepared by the U.S. EPA OAQPS regarding designing and operating flares [37]. The intent of this report is to provide guidance for predicting the performance of flares used in various industrial applications. Table G.5 in the report provides experimentally measured LFL values for mixtures containing hydrogen, methane, nitrogen, and carbon-dioxide compared to computed results. Jones et al. [38] use tables of flammability limits for carbon-monoxide, methane, and hydrogen in carbon-dioxide to develop a method to determine the mixture LFL with Le Chatelier's law. These tables were developed through multiple tests by pulling measured gas volume into an explosion tube. From there gas mixture was set to atmospheric pressure and as the tube was opened, the mixture was exposed to a flame. By adjusting the volume of the gas mixture to the amount of air in the tube, the flammability limits were determined. From there, the tables were developed and used to determine the LFL of various flammable gas and diluent mixtures.

The first step for applying this method is to split inert gas into different binned groups and combine a specified quantity with each individual combustible gas species. The tables developed by Jones give the LFL of each derived gas mixture based LFL on the ratio of combustible to inert gas. For example, if there were a mixture with 50% carbon-dioxide, 30% hydrogen and 20% methane, carbon-dioxide can be split in half and each half combined with the hydrogen and methane. This would give flammable gas to inert gas ratios of 1.2 for the hydrogen and carbon-dioxide mix and 0.8 for the methane and carbon-dioxide mix. The LFL for these flammable gas to inert gas ratios can be looked up in tables provided by Jones. The next step is to input those values into Le Chatelier's equation 1, to determine the LFL. The LFL for the binned mixtures is 9.0% for the hydrogen and carbon-dioxide mix at 55% volume percent and 10.0% for the methane and carbon-dioxide mix at 45% volume percent. This gives a mixture of LFL of 9.4% when using Equation 1. How the diluent is split according to Jones does make a difference. Using the example with 50% carbon-dioxide, 30% hydrogen and 20% methane, the percent volume of carbon-dioxide can be split and binned to equal 30% and 20%. Combining the 30% volume percent with hydrogen and 20% volume percent with methane gives and LFL of 9.8%. This is 0.4% higher than the previous binning method.

To use the method by Jones for the lithium-ion cells, it should be noted that the hydrocarbons are binned into methane. The tables used by Jones do not include other hydrocarbons. While there is some uncertainty in using this method since splitting of the diluent to combine with the combustible gas can be varied, it is used to rank or understand how flammability limit varies for each cathode chemistry. With most codes and standards

requiring the space to not allow the gas concentration to reach 25% of LFL, this safety factor will help mitigate uncertainties. The EPA paper shows a less than 10% error compared with experimental results. It is also shown that when the hydrogen amount is relatively low compared to the total combustibles, roughly 33% or less, the predicted LFL is higher than the actual LFL. This is due to the enhancement in combustion from hydrogen. Most of the vent gas compositions at 100% SOC have a combustible gas composition of 35% to 50% hydrogen.

In addition to Jones' method, the CAFT method has also been modified to take into account varying adiabatic temperatures at LFL for mixtures. The study by Bounaceur et al. [39] in 2017 furthers the understanding of approaches on predicting LFL for gas mixtures with inert gases. Through this study, a step-by-step method is provided by using a modified version of the CAFT method. The adiabatic flame temperature in this study was computed using Chemkin II which is a similar program to Cantera. According to Bounaceur, hydrogen has an adiabatic temperature criterion of 629 K compared to 1417 K to 1706 K for carbon-dioxide and multiple hydrocarbons. The study shows a summation of the adiabatic temperatures, calling this T_{blend} as a simple linear approximation in addition to the CAFT method.

$$T_{\mathrm{L,blend}} = \sum_{i=1}^{fuels} \alpha_{\mathrm{i}} T_{\mathrm{L,i}} \tag{3}$$

Equation 3 is the summation of the adiabatic flame temperatures, $T_{L,blend}$, scaled by the mole fraction of fuel, α_i. According to Bounaceur, the method has an uncertainty of about 15 K. By estimating the blended adiabatic temperature in addition to using the CAFT method, an additional method to estimating the LFL of inert, hydrogen, carbon-monoxide and hydrocarbons have been established.

2.1.1 LFL Validation

Additional work from studies such as the thesis by Terpstra et al. [40] in 2012 or the dissertation by Hai Le et al. [35] in 2013 show that even with research nearly 100 years ago there is still a gap in the overall understanding of LFL estimations. One prescribed methodology to measure the LFL is ASTM E681 Standard Test Method for Concentration Limits of Flammability of Chemicals [41]. Research by Kim et al. [42] shows that determining the LFL via testing methods such as E681 has a large uncertainty as shown in the lack of reproducibility. With the safety community relying on models to predict behaviors such as laminar flame speed, adiabatic flame temperature and maximum-overpressure, models for estimating LFL should be further studied to reduce reliance on testing.

Table 2: EPA Gas Mixtures

	Mixture 1	**Mixture 2**	**Mixture 3**
carbon-dioxide	60.6	68.4	69.8
Methane	29.0	21.1	15.1
Hydrogen	10.4	10.5	15.1

The three different mixtures used in this comparison are referred to in the EPA Flares report in table G.5 [37] are provided in Table 2 above.

Table 3: Validating LFL Calculation Methods with EPA Table

Mixture 1	**Tabulated Value**	**% Error**	**Mixture 2**	**Tabulated Value**	**% Error**	**Mixture 3**	**Tabulated Value**	**% Error**
Experimental	13.2	-	**Experimental**	15.9	-	**Experimental**	16.4	-
Le Chatelier's	11.9	10.9	**Le Chatelier's**	14.6	9.1	**Le Chatelier's**	14.7	11.6
CAFT	17.9	26.3	**CAFT**	24.3	34.4	**CAFT**	29.4	44.2
Jones	12.7	3.9	**Jones**	15.9	0.2	**Jones**	16.1	1.9
Bounaceur's	12.6	4.8	**Bounaceur's**	15.7	1.5	**Bounaceur's**	16	2.6

Table 3 compares the various methods described to calculate LFL in percent volume comparing the various gas mixtures from Table 2. It is clear by using the method provided by Jones to use a modified gas mixture prior to inputting the LFL values into Equation 1 based takes into account the diluents. This shows with a very small percent error between the experimental data. The method by Jones has an error of less than 5% while Le Chatelier's is much higher near 10%. One issue with the method by Jones is the fact that the binned compositions are up to the user. In this case, the diluent was binned equally with each flammable gas. How the

user completes this binning will influence the outcome and uncertainty. Yet this method shows results that are very close to experimental data, as seen in the EPA flare paper and Table 3 above. Also, the method by Jones is simple compared with some other methodologies and can be performed with spreadsheets.

As discussed previously, using the constant adiabatic flame temperature method has a high error due to hydrogen having a lower flame temperature compared to hydrocarbons. This is validated, as the error using the CAFT method is 26% to 44%. The method by Bounaceur using the adiabatic mixing of the fuels gives results very similar to Jones. The error with this method is just slightly higher than Jones and compared to the CAFT method it takes into account the hydrogen issues by scaling the adiabatic flame temperature. Both Jones and Bounaceur use modified versions of the known LFL computations in order to account for inert diluents and mixing hydrogen with hydrocarbons and carbon-dioxide.

The methods reviewed show two well-known methods to estimate LFL: Le Chatelier's Law and CAFT. While both methods have low uncertainty in specific applications, the battery vent gas includes hydrocarbons, hydrogen, carbon-monoxide, and inert diluents. Modified versions of these methods were used to validate with experimental data to determine if they are appropriate for lithium-ion cell vent gas. Based on the lower error in predicting experimental tests, the Jones and Bounaceur methods are the recommended methods to compute LFL for battery vent gas compositions.

2.2 Laminar Flame Speed

The second metric is the laminar flame speed for the vent gas. A cell that has undergone thermal runaway can vent a flammable mixture. Often, the cell is sufficiently hot that the vented gases ignite as a flame. Depending on whether the atmosphere contains a flammable mixture, the flame can burn in either a nonpremixed or premixed mode. The explosion hazard scenario occurs when the vented gases burn in a premixed mode. The critical parameter controlling the rate of pressurization is the burning speed. The burning speed is correlated to a fundamental flame propagation rate called the laminar flame speed (S_L). This flame speed generally increases with increasing temperature and decreases with increasing pressure.

A 1-D premixed flame can be characterized by the composition (e.g., mass fraction of the species (Y_i), pressure (P), density (ρ), and temperature (T) of the unburned mixture). As the unburned mixture reacts, the temperature increases and a propagation front evolves. Simplified governing equations are described below [43] for a steady state, 1-D, adiabatic premixed flame:

$$\dot{m}'' = \dot{m}/A = \rho v = constant \tag{4}$$

Equation 4 is mass conservation. The product of the mixture velocity, v, and the density, ρ, is the mass flux (kg/m^2-s).

$$\dot{m}''\frac{dY_i}{dx} - \rho D\frac{d^2Y_i}{dx^2} - \dot{\omega}_i''' = 0 \tag{5}$$

Equation 5 is species conservation. A simple Fick's law diffusion model is shown in which D is the diffusivity of the mixture and the volumetric source term is $\dot{\omega}'''$. For the simplest models, the volumetric source is specified in an Arrhenius form with A' being a pre-exponential factor and E_a being the activation energy.

$$\dot{m}''c_p\frac{dT}{dx} - k\frac{d^2T}{dx^2} - \dot{\omega}'''Q = 0 \tag{6}$$

Equation 6 is energy conservation. The specific heat for the mixture is c_p, k is the mixture conductivity, and Q is the heat released per mass of reactant consumed.

An approximate analytical solution for this system of equations can be found [43]:

$$S_L \approx \left[2\alpha\frac{A'}{\rho_0}exp\left(-\frac{E_a}{R_uT_f}\right)\frac{R_uT_f^2}{E_a(T_f - T_u)}\right]^{1/2} \tag{7}$$

Equation 7 describes qualitatively the flame speed, where $\alpha = k/\rho_0 c_p$ which is the thermal diffusivity, T_f is the adiabatic flame temperature, T_u is the unburned gas temperature.

The "mixture strength" is often specified using the equivalence ratio. It is the mass ratio of fuel to air compared to the stoichiometric mass ratio of fuel to air. Flammability limits can be expressed in terms of the equivalence ratio and near unity for the equivalence ratio identifies flammable mixtures with the highest adiabatic flame temperature and largest laminar flame speeds [44]. The equivalence ratio is defined as follows :

$$\Phi = \frac{\text{Fuel-to-Air-Ratio}}{\text{Stoichiometric-Fuel-to-Air-Ratio}} \tag{8}$$

There are simplified correlations for estimating the laminar flame speed that have been used and studied. For example, the laminar flame speed can be estimated for some hydrocarbons as follows [45] :

$$S_L(T,P) = S_{L,ref}\left(\frac{T_u}{T_{u,ref}}\right)^m \left(\frac{P}{P_{ref}}\right)^n (1 - 2.1Y_{dil}) \tag{9}$$

Where T_u and P are the unburned gas temperature and pressure and m and n are constants. The diluent mass fraction is Y_{dil}. Equation 9 shows that increasing the amount of diluent gas reduces the flame speed. The reference laminar flame speed is specified by the fuel composition and equivalence ratio. As previously noted, this flame speed is an essential input to understand the explosion hazard and for calculating vent requirements needed to reduce explosion pressures.

2.2.1 Laminar Flame Speed Validation

Laminar flame speeds are typically measured using either combustion bombs or flat flame burners. Critical issues in measuring laminar flame speeds are correcting for heat losses and flame curvature/strain rate. Uncertainties in these measurements are typically on the order of 15% for stoichiometric mixtures and larger for near limit conditions.

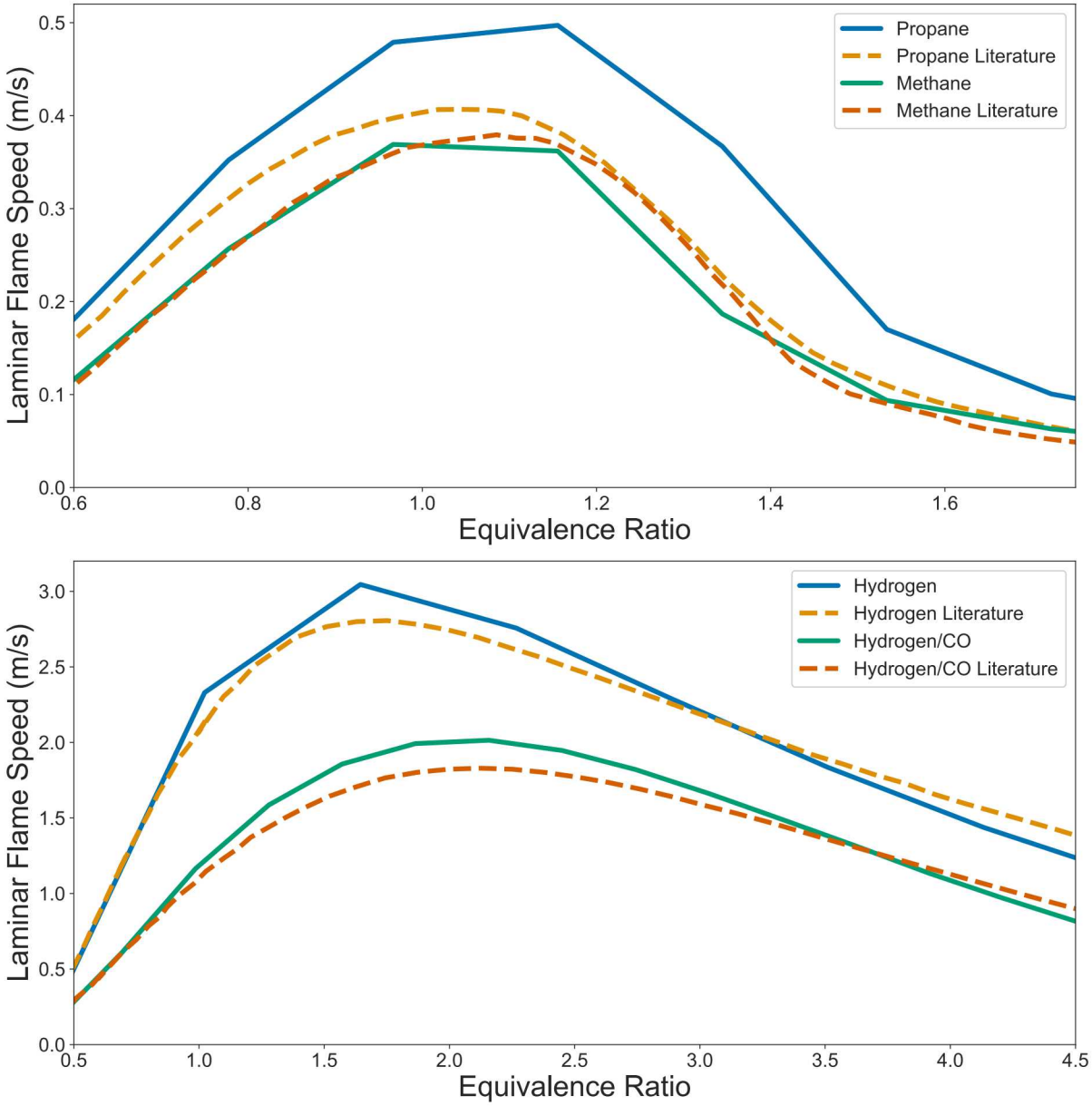

Figure 2: Cantera Model Verification with Literature

The results from Figure 2 show the computed laminar flame speeds for propane and methane from Cantera compared with literature values Dirrenberger et al. [46] along with hydrogen and a hydrogen/carbon-monoxide mixture from Cantera compared with literature values by Krejci et al. [47] and Dirrenberger et al. [46]. The temperature and pressure were set at 300 Kelvin and one atmosphere for the model.

Table 4: Maximum Flame Speed Comparison

Max Flame Speed (cm/s)	**Propane**	**Methane**	**Hydrogen**	**Hydrogen/CO**
Literature	0.41	0.38	2.81	1.83
Computed	0.50	0.37	3.05	2.01
Percent Difference (%)	22.21	2.73	8.53	10.12

The study by Krejci et al. [47] gives the uncertainty of the measurements of the laminar flame speed. Depending on the equivalence ratio, an uncertainty of ± 6.9 cm/s to ± 7.4 cm/s was found for a hydrogen and air mixture. Additionally, Chen et al. [48] reviewed the accuracy of flame speed measurements and showed the multiple tests have different flame speed curves based on the testing apparatus. Comparing the computed

values for methane compared to the literature values, there is almost no deviation in the two. Only once the equivalence ratio is above 1.20 do the flame speeds vary slightly, but the difference is small. When comparing propane in the same fashion, there is a more obvious deviation between the two. Figure 2 shows that the laminar flame speed for propane is slightly higher than the literature values by about 6-10 cm/s. Yet when looking at the overall compositions of the battery vent gas from 1, with the hydrocarbons only taking up about 15% to 25% of the composition by volume and propane only taking up a fraction of that volume, this is not expected to be a significant effect. Also, when comparing with other literature that had used Cantera such as Johnsplass et al. [49], the propane flame speed compared with the study are very similar in terms of peak flame speeds. Similarly, the hydrogen and carbon-monoxide mixture model is slightly higher than the literature, but again only by about 25 cm/s at the peak. The peak flame speeds are well above the 250 cm/s. It should be noted that hydrogen has a much higher flame speed than propane and methane, which will be discussed when comparing different battery vent gas compositions. Overall, all the literature reviews show close comparisons with the models from Cantera. Propane is the only main species with a moderately large deviation from the literature, but with such a small volume fraction and the sensitivity study not showing a major difference in the binning method, the effects are considered to be small.

When comparing the literature for different flame speeds of higher order hydrocarbons [50, 51, 46], it can be noted that n-butane, n-pentane, and toluene have extremely similar laminar flame speed behavior when compared to propane. It appears that each of the different higher-level hydrocarbons has similar properties. Also, many of the higher order hydrocarbon species in the original compositions are of a small percentage by volume. This gives a basis behind 'binning' the original species not included in GRI-Mech into propane. To ensure that this assumption was valid, a sensitivity study was performed by varying the 'binned' species across from 100% propane to 100% methane and a 50/50 mixture by volume. Each case showed a maximum difference of 1 cm/s at the peak flame speed when comparing the propane to the methane mixture. This difference is small when the peak is almost 50 cm/s overall.

2.3 Vented Enclosure Explosion Model

To determine the consequences of an indoor explosion in terms of pressure-time history, a vented enclosure explosion model is needed. This model relies on both properties of the gas mixture and the geometry and venting of the enclosure. Key gas property inputs are laminar flame speed and maximum constant-volume adiabatic pressure or Pmax.

P_{max} is the pressure that is generated when the gas is combusted in a perfectly adiabatic, constant volume process. This pressure defines the maximum possible pressure that the gas could possibly generate. Cantera uses thermodynamic properties of the mixture to calculate P_{max}. P_{max} depends on the final composition of species produced after combustion and the adiabatic flame temperature.

Once the properties of the flammable gas mixture such as flame speed and maximum pressure are known, a vented enclosure explosion model can be used to predict explosion severity for a given gas mixture and geometry. In this study, a simple model is used to calculate the pressure time history produced by deflagrations of flammable gas mixtures.

The vented enclosure explosion model was developed by Atomic Energy of Canada [52] and has later been implemented by others [53, 54]. The model is a 0D physics model based on burning rate and conservation of momentum and energy. The model assumes that the gases are premixed, homogeneous, ideal gases. The properties of the burnt and unburnt mixtures are assumed to be spatially uniform. The model assumes an infinitely thin, smooth flame front. Burning is assumed to be slow such that the pressure in the volume is spatially uniform but temporally evolving. Compression and expansion of the unburnt mixture are isentropic. The model consists of three ordinary differential equations which are solved simultaneously.

The first equation is the conservation of mass. In this equation m_i is the initial mass of unburned gas, m_u is the mass of unburned gas, m_v is the mass of the vented gas and n is the ratio of the mass of burned gas to the initial mass.

$$\frac{d}{dt}\left(\frac{m_u}{m_i}\right) + \frac{d}{dt}(n) + \frac{d}{dt}\left(\frac{m_v}{m_i}\right) = 0 \tag{10}$$

The conservation of energy equation is similar, where E_b is the energy of the burned mixture and E_u is the

energy of the unburned mixture.

$$\frac{d}{dt}\left(\frac{m_u}{m_i}E_u\right) + \frac{d}{dt}\left(nE_b\right) + E_u\frac{d}{dt}\left(\frac{m_v}{m_i}\right) = 0 \tag{11}$$

The rate of burned gas production is based on the laminar flame speed S, and area A of the flame front and unburned gas density ρ_u.

$$\frac{dn}{dt} = \frac{1}{m_i}\rho_u SA \tag{12}$$

More details of the formulation of equations for use in the model can be found in the original paper on the model [52].

2.3.1 Explosion Model Validation

The model is validated using various experiments found in the literature. A comparison is made with experiments performed by Kumar [55] using 20% and 29.5% hydrogen mixed with air at a temperature of 373 K. For this validation, the flame speed for hydrogen is calculated using equations provided in Mulpuru et al [52]. In the experiments the pressure time history was recorded for well-mixed, centrally ignited hydrogen-air mixtures in a 6.37 m^3 spherical vessel. Model results are compared against the experiment in Figure 3. From this comparison, the maximum pressures align very well, while the predicted rise rate is slightly faster for the stoichiometric mixture of hydrogen and is a little slower for the 20% hydrogen case. The rate of pressure rise is dependent on the flame speed, which can be hard to estimate as in this sized vessel the flame speed is accelerating as temperature and turbulence increase.

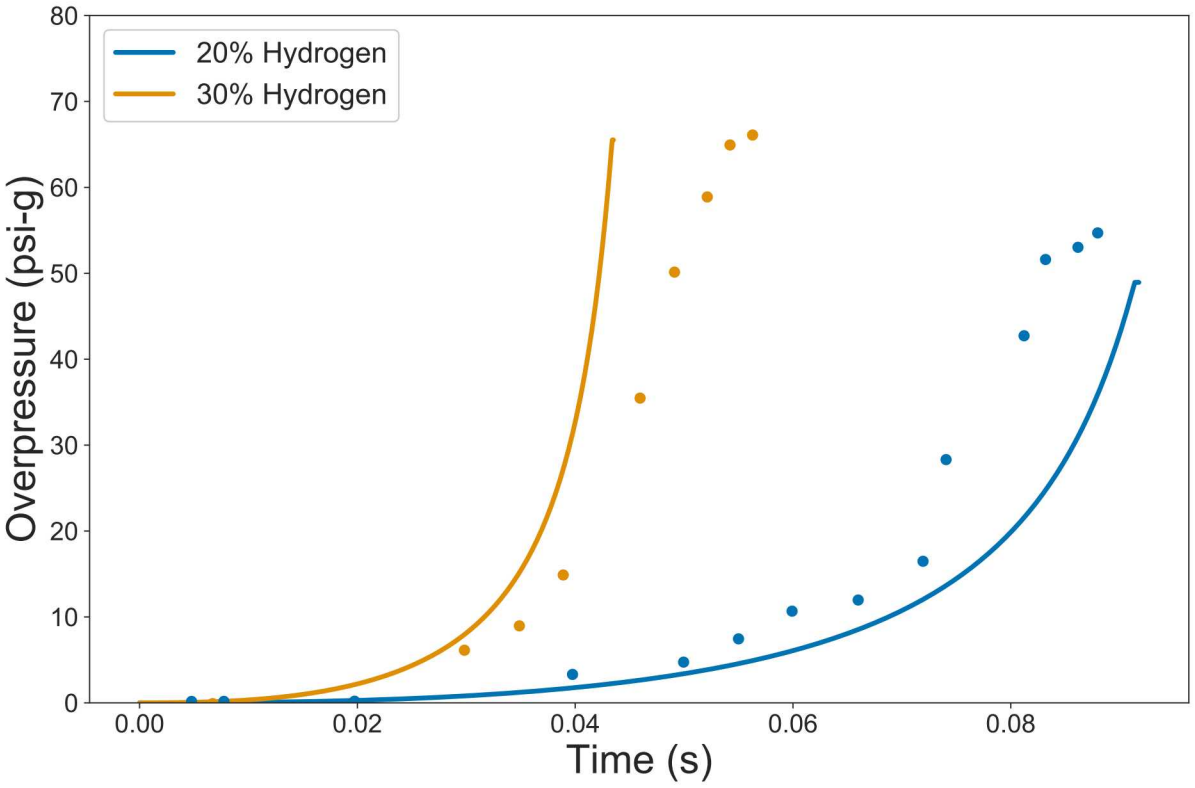

Figure 3: Model Results Compared against Experimental Data [55]

3 Results & Discussions

The models previously discussed can be used to characterize the hazard for vent gases generated from Li-BESS failure. Applying the models for LFL provides gas concentration at which a fire or explosion hazard

exists. The laminar flame speed and maximum overpressure are critical inputs for predicting explosion consequences and designing deflagration venting systems. For example, NFPA 68 Standard on Explosion Protection by Deflagration Venting Chapter 7 [56] provides prescribed methods for designing deflagration vents to reduce the consequences for gas explosions. As inputs such as the laminar flame speed and maximum overpressure increase, so does the overall vent size. In fact, the flame speed is one of the main factors for the vent size. This prescribed methodology helps gain insight into how safety systems use these metrics. As the lower flammability limit decreases, the volume of gas to reach a fire or explosion scenario decreases. As the flame speed and the maximum overpressure increase, the overall consequence of an explosion also increases.

3.1 Lower Flammability Limit

First, the various LFL models will be applied to the battery vent gas. The LFL and adiabatic temperature criteria values for the battery species comes from various literature sources such as the studies by Bounaceur et al. [39] and Vidal et al. [57]. The LFL values for each individual species are used for predicting the vent gas composition LFL with Le Chatelier's law.

Table 5: LFL and Adiabatic Criteria for Vent Gas

	CO	**H2**	**CH4**	**C2H4**	**C2H6**	**C3H8**
T_{ad} Criteria (K)	1417	629	1480	1369	1602	1509
LFL (%Volume)	12.5	4	5	2.7	3	2.1

Table 5 gives the adiabatic temperature criteria used in the method by Bounaceur et al. When comparing the LFL values obtained using the method by Jones with experimental data from Somandepalli et al., there are differences in the results. When comparing with Somandepalli, the LFL reported was 6.3% for the 100% SOC test. Yet the computed values show 8.1%. The method by Bounaceur gives a value of 8.5%. Computations for LFL using the species composition from the study by Somandepalli et al. at 100% SOC are shown in the table below:

Table 6: Comparing LFL Calculation Methods with Experimental Data

Somandepalli (2014) LCO	**Tabulated Value**	**%Error**
Experimental	6.3	-
Le Chatelier's	6.5	3.08
CAFT	10.3	38.83
Jones	8.1	22.22
Bounaceur's	5.8	-8.62

Table 6 compares the experimental data from Somandepalli with the four different methods to calculate LFL in this section. Since the method by Jones only provides tables for methane and the battery vent gas composition includes multiple hydrocarbons, this will cause uncertainty. For the other methods, any species not in Cantera are binned with propane. Since the LFL for methane is approximately 5% whereas propane has an LFL of roughly 2%, this could account for the difference in the calculated value to be higher than that of the experiment by Somandepalli. When comparing with Bounaceur's method, the results are a lot lower compared with the experimental data. The reason behind this could be the larger amount of hydrogen and carbon-monoxide compared to the other species in the vent gas composition. For the fuel composition measured from the LCO cell at 100% SOC, hydrogen is 45.7% and carbon-monoxide is 37.8% of the fuel by volume. This causes the overall mixed temperature to be 1066 K. When using the CAFT method, the prediction was a lot higher due to the high adiabatic temperature assumed. The limitation of Bounaceur's method might come when the species composition has a large volume fraction of hydrogen. In this case, Le Chatelier's method actually has the lowest error between the different methods. As shown in the dissertation by Zhao [58], based on the fuel species and the diluent volume fraction, the percent error can be low. The trends show with methane and propane blends, as the number of diluent increases, so does the percent error from the experimental value. In Table 3, with a diluent of about 60% to 70%, the error using Le Chatelier's method has a larger percent error compared to Jone's and Bounaceur's method has a much smaller error.

Table 7: LFL Predictions for Battery Vent Gas

	Le Chatelier's	**CAFT**	**Jone's**	**Bounaceur's**
LCO	6.5 to 7.5	10.3 to 13.6	8.1 to 8.8	5.8 to 8.5
LFP	8.3 to 8.7	18.2 to 20.6	9.4 to 10.0	8.6 to 8.7
NCA	6.2 to 9.8	13.7 to 16.7	6.7 to 10.9	7.6 to 11.8

Looking at Table 7, the predictions for LFL of the battery vent gas have a large range of results based on the method used. The vent gas compositions for each range is based on the tests at 100% SOC. Each method has its own set of uncertainties and constraints on how it can be applied. Clearly, the CAFT method is going to have the largest error and should not be used for hydrocarbon, hydrogen, carbon-monoxide and inert diluent mixtures. The estimated LFL is much higher than any of the other methods, as mentioned due to the hydrogen effect and adiabatic flame criteria being so much lower. By modifying the CAFT method with a mixed adiabatic temperature, Bounaceur's method is a lot more reasonable and has about the same error as Jone's method when compared with experimental data in Table 3. Le Chatelier's method works and is well known but based on the mixture the other provided methods could have a lower uncertainty.

3.2 Laminar Flame Speed

Now that the LFL ranges have been established, the laminar flame speed will be the next model to apply to the vent gases. To help validate the flame speed model even further, comparisons to a similar study by Johnsplass et al. [49] which used the data from the 2014 paper by Golubkov et al. [18]. The paper by Johnsplass used the species compositions from Golubkov to determine the laminar flame speeds as a function of the equivalence ratio using Cantera. The three flame speed plots that Johnsplass presented were compared to help further validate the model. The battery vent gas compositions were for LFP, LCO and NMC chemistries, in which the flame speed plots in this paper compared to Johnplass were very similar in terms of shape and the overall peak flame speeds. This assured that the model is similar to other studies and could be used to predict the flame speeds for other vent gas compositions.

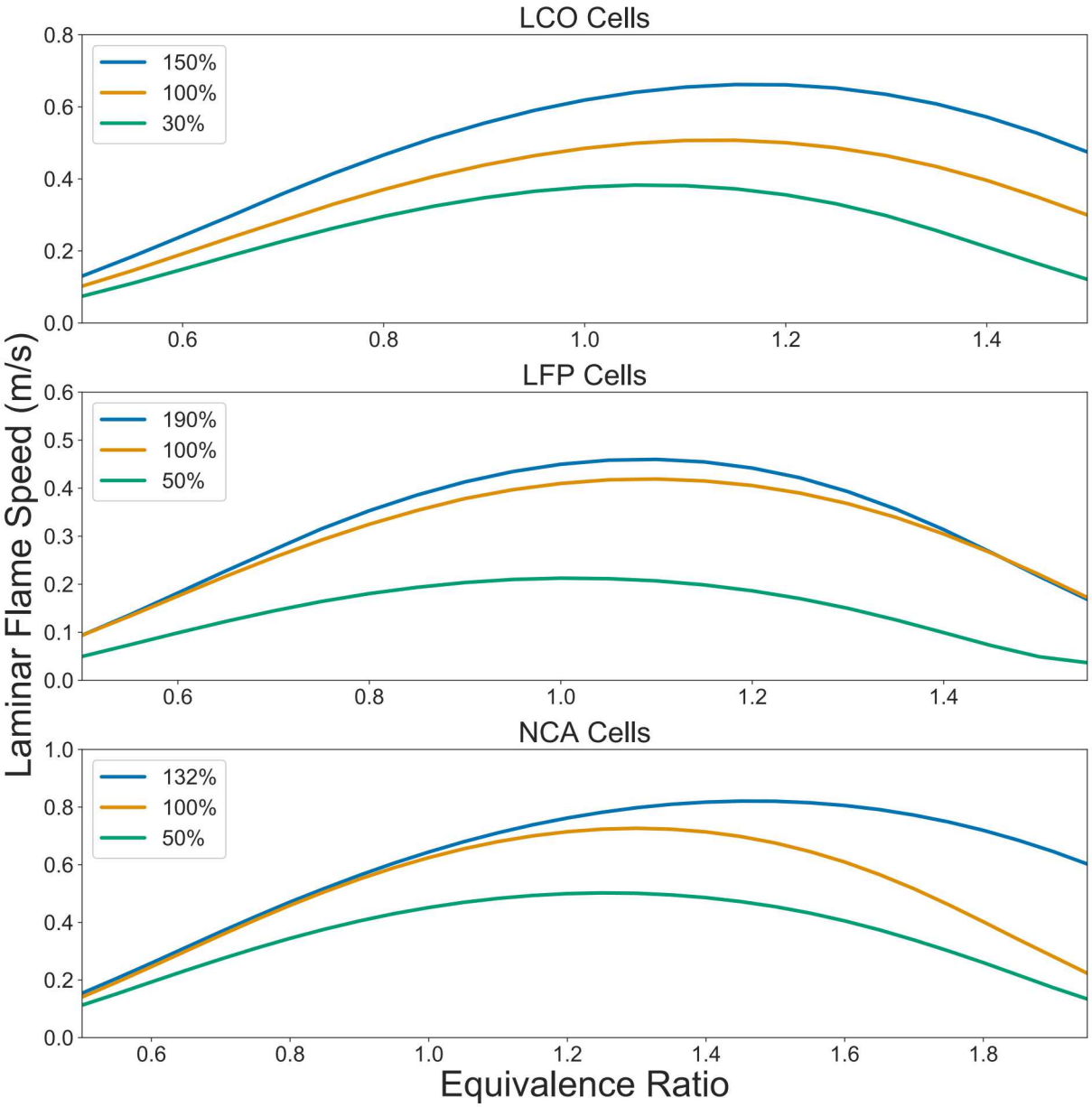

Figure 4: Laminar Flame Speed Plots by Cathode Chemistry

Figure 4 gives the laminar flame speeds at varying states of charge for battery tests for each cathode chemistry. Not all results were given, rather a range of flame speeds with increasing SOC. The results show that as the state of charge in the cell increases, the overall laminar flame speed increases. There are some interesting observations to note. The LCO cells have a peak flame speed of anywhere from 0.4 to 0.6 m/s as the SOC increases. The peak values are at an equivalence ratio of roughly 1.1. The LFP cells have a lower overall flame speed, with a peak between 0.4 and 0.5 ms/. The literature gives higher overall SOC tests when compared to the LCO batteries in which there are only two sets of data with a cell over 100% SOC. By referring to Figure 1, it can be seen that the volume fraction of carbon-dioxide in the vent gas composition begins to increase with the SOC for LFP cells. This is possibly why at higher SOC the flame speeds are not increasing to the range of the other cells. Lastly, the NCA cells have the highest overall flame speed between 0.6 to 0.8 for the peaks at an equivalence ratio of 1.2 to 1.4. This can directly be linked to an increased amount of hydrogen and much less carbon-dioxide in the vent gas compositions for the NCA batteries.

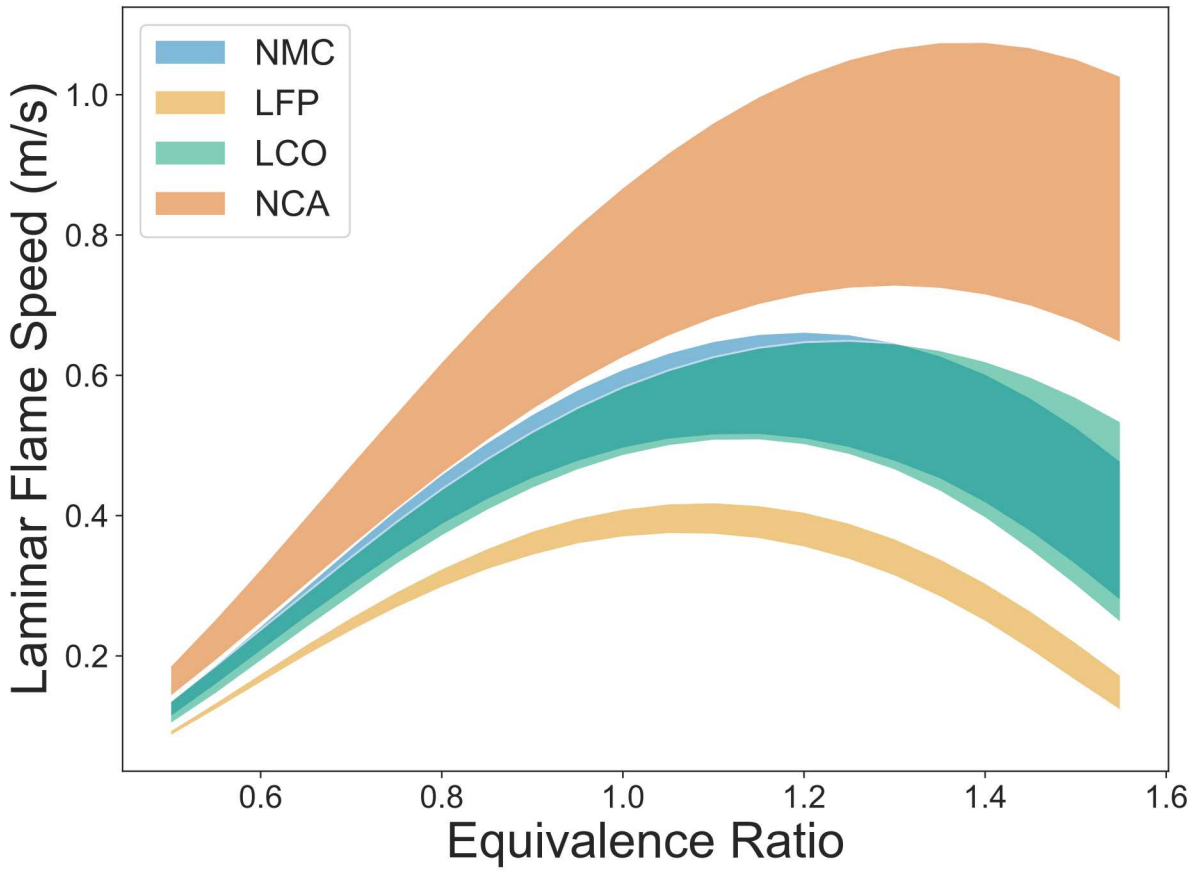

Figure 5: Laminar Flame Speed Ranges by Cathode Chemistry at 100 % SOC

Figure 5 shows the range of flame speeds at 100% SOC for varying chemistries. This figure clearly shows a large difference in the flame speeds for different chemistries at the same SOC. While flammable gas hazards are mainly based on the concentration in a space, the results from the flame speed model show that understanding the specific cell state of charge, construction type, chemistry, and capacity. This also shows that NCA cells clearly have a larger flame speed, but with such a larger range there is a need to further understand how differences in construction and capacity effect these values.

3.3 Explosion Pressures

The adiabatic constant volume maximum pressure was calculated using Cantera to compare with experimental data. Somandapelli et al. mixed battery vent gas with air at different equivalence ratios and measured the peak overpressure as well as the peak rate of pressure rise in a 20L spherical vessel [17]. Cantera was run using a variety of different fuel concentrations to evaluate the impact of different mixtures with air. Values for maximum pressure calculated using Cantera are compared to experimental data in Figure 6.

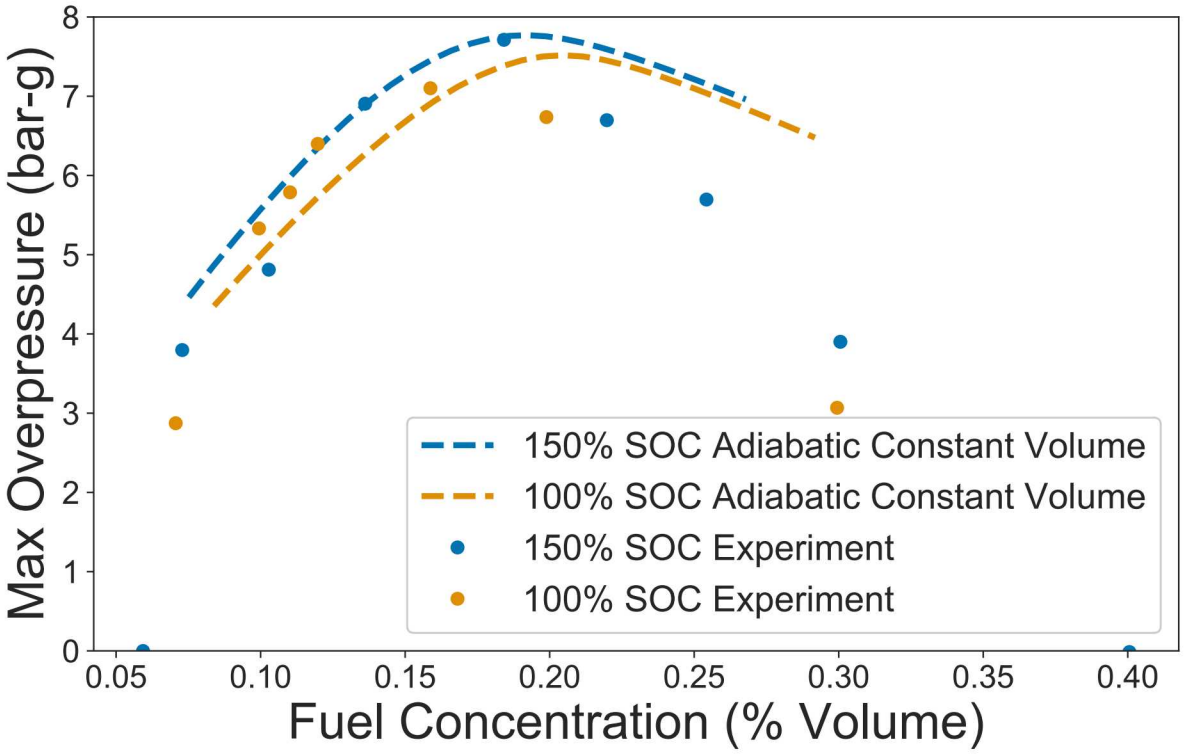

Figure 6: Maximum Overpressure Model Data Compared against Experimental Data [17]

Using the same technique as above with different compositions of battery vent gas, ranges of possible maximum pressure were determined. Figure 7 shows the range of pressure for the maximum pressure at 100% SOC for varying chemistries. The maximum overpressure values for different chemistries show less of a variation than the laminar flame speed models. As with the laminar flame speeds, the maximum over-pressure is lower for the LFP cells compared with the NCA and LCO cells. Also, for the equivalence ratio of between 1 and 1.2, the mixtures produces the highest maximum overpressures.

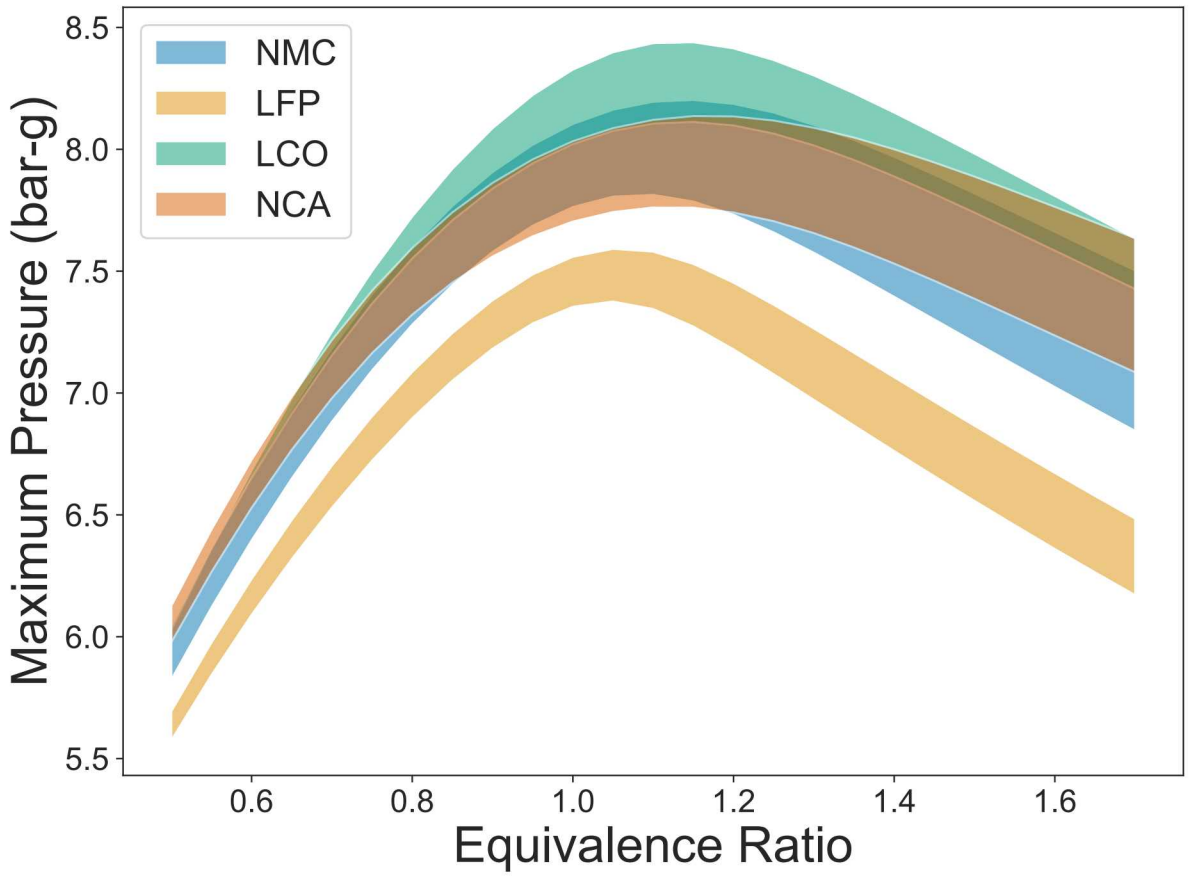

Figure 7: Maximum Overpressure Ranges by Cathode Chemistry at 100% SOC

Another important parameter for the analysis of explosion scenarios is the rate of pressure rise. The rate of pressure rise is usually compared using the parameter Kg, which is calculated using the maximum rate of pressure rise $\frac{dp}{dt}$ and the volume V as shown below.

$$K_g = \frac{dp}{dt} V^{\frac{1}{3}} \tag{13}$$

The value of K_g was previously used in NFPA 68 to inform the sizing of deflagration vents. The Kg value developed using the model is compared to results from experiments as shown in Figure 8.

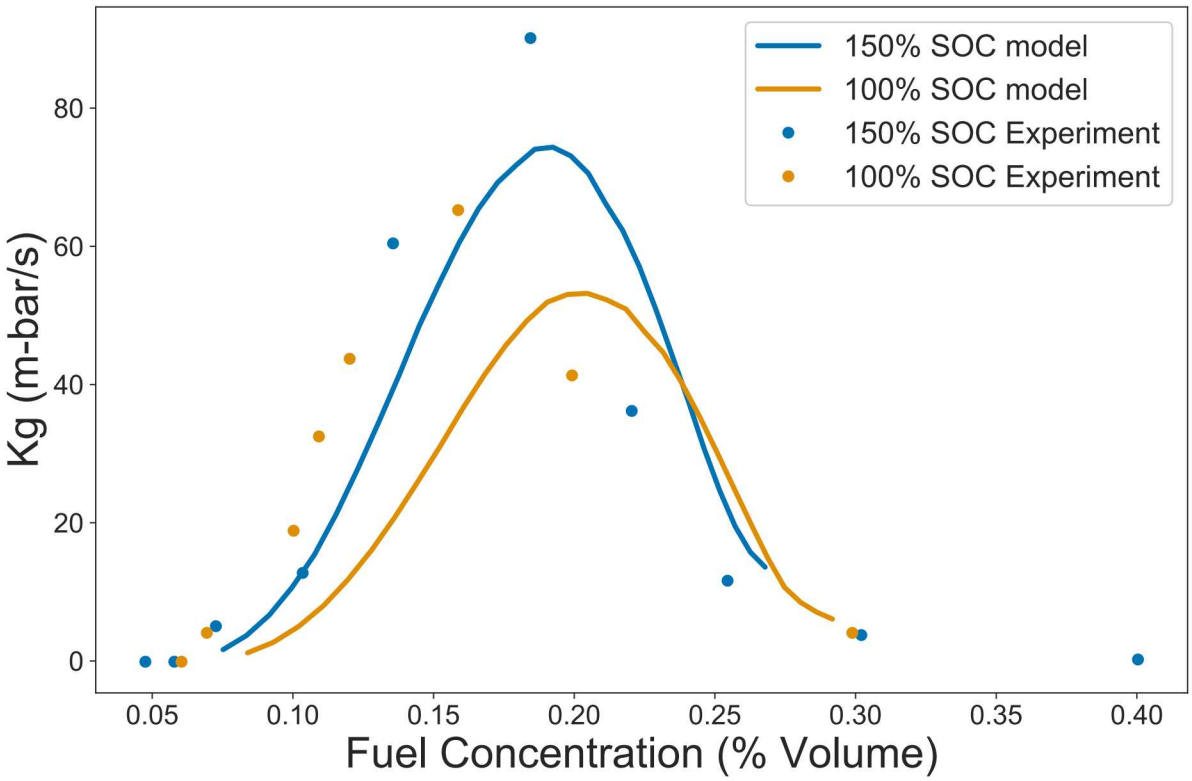

Figure 8: K_g Model Data Compared against Experimental Data [17]

The predicted maximum K_g values from the model are 17-18 % less than the experiment values from the literature. This is due to the assumption in the model that the flame propagates at the laminar flame speed and neglects flame acceleration due to turbulence or temperature increases. Overall the trend of Kg with varying fuel concentration seems to match that seen in the experiments.

3.4 Ranking Vent Gas Hazards

It has been established from prescribed codes such as NFPA 1 Chapter 52 that as the LFL decreases the overall hazard increases. From NFPA 68 Chapter 7 its as the laminar flame speed and maximum overpressure increases, so do the safety requirements. Applying the models for these three metrics to the battery vent gas provides a method to establish and rank the hazard of the vent gas.

Table 8: Range of Battery Cell Model Results at 100% SOC

Cell Chemistry	Lower Flammability Limit (%)	Peak Laminar Flame Speed (m/s)	Maximum Over-Pressure (bar-g)
LCO	5.8 to 8.8	0.50 to 0.66	7.81 to 8.44
LFP	8.6 to 10.0	0.37 to 0.42	7.38 to 7.60
NCA	6.7 to 11.8	0.69 to 1.07	7.74 to 8.13

Table 8 shows the range for LFL, maximum flame speed, and maximum overpressure. LFL values are presented taking the minimum and maximum values from the method by Jones and Bounaceur to establish a range. The values for the flame speed and maximum overpressure are displayed for the equivalence ratio which the maximum flame speed occurs to quantify the hazards of each cell chemistry.

The results overall show that the LFP cell vent gas generally has a higher flammability limit at 100% SOC, which allows more gas to accumulate before reaching a deflagration or fire hazard compared with the NCA or LCO cells. The NCA cells do have one instance where the LFL is higher at 100% SOC, which is the results from Lammer (2017) as seen in Figure 1 which has a higher amount of carbon-dioxide compared to the other

NCA vent gas compositions. The LFP battery vent gas also has a lower overall maximum overpressure and laminar flame speed. This is important when considering safety as both values increase, so does the associated hazard and consequence.

Overall, each cell chemistry vent gas has a similar amount of hydrocarbons produced shown in Figure 1. Comparing with the LCO and LFP cells, the NCA cells have a higher concentration of hydrogen by volume and much less carbon-dioxide, which is an inert diluent. The LCO vent gas has less carbon-dioxide than LFP vent gas overall, yet a larger amount carbon-monoxide and hydrocarbons by volume. These observations can be directly associated with the higher flame speed and maximum overpressure shown in the results for NCA and LCO from the effects of hydrogen compared with methane or other hydrocarbons. This directly correlates into the NCA and LCO cells having a higher quantifiable level of hazard compared with the LFP cells when comparing all the models.

With the electrical energy density of NCA and LCO cells being higher gives the benefit of a lower overall system weight compared to the LFP cells as shown by Wu et al. [59]. Yet with higher overpressure and flame speeds, the module and rack safety systems should be designed to accommodate the deflagration hazard based on the cell chemistry. To compensate for higher potential burst damage from NCA cells, the module and rack designs may change with heavier duty and thicker materials. Using this approach will potentially cause reconsideration in industries such as aerospace where weight is a large factor if the electrical energy density is measured with the safety systems.

4 Conclusions

This paper presents a review of battery vent gas compositions for various chemistries and SOC. The critical models used to estimate LFL, laminar flame speed, and maximum overpressure are discussed and guidance is provided on how these models can be used to predict vent gas combustion properties. All the analyses were completed using methodology and tools that are freely available. This gives the ability for the safety community to design systems based on their own data. These models were applied to literature aggregated data of cell vent gases. The combustion metrics that were evaluated show that NCA and LCO vented gases produce higher flame speeds and maximum overpressures relative to LFP vent gases. LFP cells also have a higher LFL, which likely reduces the probability of a flammable ignition.

The findings reported here are based on literature gas compositions from numerous experiments performed over two decades. The experiments vary with cell chemistry, electrolyte, form factor, manufacturer, failure mode, cell capacity, SOC and experimental setup. This review shows the need for further gas composition experiments to better characterize gas release from cells. In most cases, the gas composition for a given SOC and chemistry is only measured in one or two experiments. Parameters of interest such as LFL, laminar flame speed and maximum overpressure have been measured in very few experiments. This indicates the need for additional testing to further validate the models. As more testing is completed to understand the species composition along with the gas production and rates at the cell, module and rack levels, more data will be available to further understand hazards and technologies to mitigate these hazards.

References

[1] K. Staff, "Neighborhood residents concerned following train car explosion," Apr. 2017. [Online]. Available: https://www.khou.com/article/news/local/neighborhood-residents-concerned-following-train-car-explosion/285-433810198

[2] S. Beausoleil, "Lithium batteries causes train car explosion in NE Houston," Apr. 2017. [Online]. Available: https://www.click2houston.com/news/train-catches-fire-in-ne-houston

[3] J. Deign, "Engie Investigates Source of Belgian Battery Blaze," Dec. 2017. [Online]. Available: https://www.greentechmedia.com/articles/read/engie-investigates-source-of-belgian-battery-blaze

[4] N. Hyun-woo, "Frequent fire raising concerns over safety of solar energy," Jan. 2019. [Online]. Available: https://www.koreatimes.co.kr/www/tech/2018/12/133_260560.html

[5] "Injured firefighters identified from substation battery explosion in Surprise | Arizona News | azfamily.com." [Online]. Available: https://www.azfamily.com/news/firefighters-hospitalized-after-power-substation-battery-explosion-in-surprise/article_c28a7f1e-631c-11e9-9bf1-bfa00f273619.html

[6] "Eight AZ Firefighters Hurt, One Critically, in Explosion." [Online]. Available: https://www.firehouse.com/safety-health/news/21077221/eight-az-firefighters-injured-one-critically-in-a-large-utility-battery-explosion

[7] H. Mai, "APS storage facility explosion raises questions about battery safety," Apr. 2019. [Online]. Available: https://www.utilitydive.com/news/aps-storage-facility-explosion-raises-questions-about-battery-safety/553540/

[8] "NFPA 1: Fire Code." [Online]. Available: https://www.nfpa.org/codes-and-standards/all-codes-and-standards/list-of-codes-and-standards/detail?code=1

[9] "NFPA 855: Standard for the Installation of Stationary Energy Storage Systems." [Online]. Available: https://www.nfpa.org/codes-and-standards/all-codes-and-standards/list-of-codes-and-standards/detail?code=855

[10] K. Kumai, H. Miyashiro, Y. Kobayashi, K. Takei, and R. Ishikawa, "Gas generation mechanism due to electrolyte decomposition in commercial lithium-ion cell," *Journal of Power Sources*, vol. 81-82, pp. 715–719, Sep. 1999. [Online]. Available: http://linkinghub.elsevier.com/retrieve/pii/S0378775398002341

[11] T. Ohsaki, T. Kishi, T. Kuboki, N. Takami, N. Shimura, Y. Sato, M. Sekino, and A. Satoh, "Overcharge reaction of lithium-ion batteries," *Journal of Power Sources*, vol. 146, no. 1-2, pp. 97–100, Aug. 2005. [Online]. Available: http://linkinghub.elsevier.com/retrieve/pii/S0378775305005112

[12] W. Kong, H. Li, X. Huang, and L. Chen, "Gas evolution behaviors for several cathode materials in lithium-ion batteries," *Journal of Power Sources*, vol. 142, no. 1, pp. 285–291, Mar. 2005. [Online]. Available: http://www.sciencedirect.com/science/article/pii/S037877530401078X

[13] D. H. Doughty, E. P. Roth, C. C. Crafts, G. Nagasubramanian, G. Henriksen, and K. Amine, "Effects of additives on thermal stability of Li ion cells," *Journal of Power Sources*, vol. 146, no. 1, pp. 116–120, Aug. 2005. [Online]. Available: http://www.sciencedirect.com/science/article/pii/S0378775305005057

[14] D. Abraham, E. Roth, R. Kostecki, K. McCarthy, S. MacLaren, and D. Doughty, "Diagnostic examination of thermally abused high-power lithium-ion cells," *Journal of Power Sources*, vol. 161, no. 1, pp. 648–657, Oct. 2006. [Online]. Available: https://linkinghub.elsevier.com/retrieve/pii/S0378775306006768

[15] E. P. Roth, "Abuse Response of 18650 Li-Ion Cells with Different Cathodes Using EC:EMC/LiPF6 and EC:PC:DMC/LiPF6 Electrolytes," *ECS Transactions*, vol. 11, no. 19, pp. 19–41, Mar. 2008. [Online]. Available: http://ecst.ecsdl.org/content/11/19/19

[16] P. Ribière, S. Grugeon, M. Morcrette, S. Boyanov, S. Laruelle, and G. Marlair, "Investigation on the fire-induced hazards of Li-ion battery cells by fire calorimetry," *Energy & Environmental Science*, vol. 5, no. 1, pp. 5271–5280, Jan. 2012. [Online]. Available: http://pubs.rsc.org/en/content/articlelanding/2012/ee/c1ee02218k

[17] V. Somandepalli, K. Marr, and Q. Horn, "Quantification of Combustion Hazards of Thermal Runaway Failures in Lithium-Ion Batteries," *SAE Int. J. Alt. Power.*, vol. 3, no. 1, pp. 98–104, May 2014.

[18] A. W. Golubkov, D. Fuchs, J. Wagner, H. Wiltsche, C. Stangl, G. Fauler, G. Voitic, A. Thaler, and V. Hacker, "Thermal-runaway experiments on consumer Li-ion batteries with metal-oxide and olivin-type cathodes," *RSC Advances*, vol. 4, no. 7, pp. 3633–3642, 2014. [Online]. Available: https://pubs.rsc.org/en/content/articlelanding/2014/ra/c3ra45748f

[19] F. Larsson, P. Andersson, P. Blomqvist, A. Lorén, and B.-E. Mellander, "Characteristics of lithium-ion batteries during fire tests," *Journal of Power Sources*, vol. 271, pp. 414–420, Dec. 2014. [Online]. Available: http://www.sciencedirect.com/science/article/pii/S0378775314012828

[20] N. S. Spinner, C. R. Field, M. H. Hammond, B. A. Williams, K. M. Myers, A. L. Lubrano, S. L. Rose-Pehrsson, and S. G. Tuttle, "Physical and chemical analysis of lithium-ion battery cell-to-cell failure events inside custom fire chamber," *Journal of Power Sources*, vol. 279, pp. 713–721, Apr. 2015. [Online]. Available: http://www.sciencedirect.com/science/article/pii/S0378775315000804

[21] Y. Fu, S. Lu, K. Li, C. Liu, X. Cheng, and H. Zhang, "An experimental study on burning behaviors of 18650 lithium ion batteries using a cone calorimeter," *Journal of Power Sources*, vol. 273, pp. 216–222, Jan. 2015. [Online]. Available: http://www.sciencedirect.com/science/article/pii/S0378775314014475

[22] Q. Yuan, F. Zhao, W. Wang, Y. Zhao, Z. Liang, and D. Yan, "Overcharge failure investigation of lithium-ion batteries," *Electrochimica Acta*, vol. 178, pp. 682–688, Oct. 2015. [Online]. Available: http://www.sciencedirect.com/science/article/pii/S0013468615302140

[23] A. W. Golubkov, S. Scheikl, R. Planteu, G. Voitic, H. Wiltsche, C. Stangl, G. Fauler, A. Thaler, and V. Hacker, "Thermal runaway of commercial 18650 Li-ion batteries with LFP and NCA cathodes – impact of state of charge and overcharge," *RSC Advances*, vol. 5, no. 70, pp. 57 171–57 186, Jun. 2015. [Online]. Available: http://pubs.rsc.org/en/content/articlelanding/2015/ra/c5ra05897j

[24] J. Sun, J. Li, T. Zhou, K. Yang, S. Wei, N. Tang, N. Dang, H. Li, X. Qiu, and L. Chen, "Toxicity, a serious concern of thermal runaway from commercial Li-ion battery," *Nano Energy*, vol. 27, pp. 313–319, Sep. 2016. [Online]. Available: http://www.sciencedirect.com/science/article/pii/S2211285516302130

[25] Y. Zheng, K. Qian, D. Luo, Y. Li, Q. Lu, B. Li, Y.-B. He, X. Wang, J. Li, and F. Kang, "Influence of over-discharge on the lifetime and performance of LiFePO4/graphite batteries," *RSC Advances*, vol. 6, no. 36, pp. 30 474–30 483, Mar. 2016. [Online]. Available: http://pubs.rsc.org/en/content/articlelanding/2016/ra/c6ra01677d

[26] T. Maloney, "Home : FAA Fire Safety," Oct. 2016. [Online]. Available: https://www.fire.tc.faa.gov/systems/lithium-batteries

[27] M. Lammer, A. Königseder, and V. Hacker, "Holistic methodology for characterisation of the thermally induced failure of commercially available 18650 lithium ion cells," *RSC Advances*, vol. 7, no. 39, pp. 24 425–24 429, May 2017. [Online]. Available: http://pubs.rsc.org/en/content/articlelanding/2017/ra/c7ra02635h

[28] F. Larsson, P. Andersson, P. Blomqvist, and B.-E. Mellander, "Toxic fluoride gas emissions from lithium-ion battery fires," *Scientific Reports*, vol. 7, no. 1, pp. 1–13, Aug. 2017. [Online]. Available: https://doaj.org

[29] Y. Fernandes, A. Bry, and S. de Persis, "Identification and quantification of gases emitted during abuse tests by overcharge of a commercial Li-ion battery," *Journal of Power Sources*, vol. 389, pp. 106–119, Jun. 2018. [Online]. Available: https://linkinghub.elsevier.com/retrieve/pii/S0378775318302581

[30] D. G. Goodwin, H. K. Moffat, and R. L. Speth, "Cantera: An Object-Oriented Software Toolkit For Chemical Kinetics, Thermodynamics, And Transport Processes. Version 2.3.0," Jan. 2017. [Online]. Available: https://zenodo.org/record/170284

[31] M. Frenklach, T. Bowman, and G. Smith, "GRI-MECH." [Online]. Available: http://www.me.berkeley.edu/gri_mech/

[32] H. Le Chatelier, "Estimation of firedamp by flammability limits," *Annals of Mines*, vol. 19, no. 8, pp. 388–395, 1891.

[33] J. G. Quintiere, "Fundamentals of Fire Phenomena," in *Fundamentals of Fire Phenomena*. John Wiley & Sons, 2006, pp. 77–115.

[34] I. A. Zlochower, "Experimental flammability limits and associated theoretical flame temperatures as a tool for predicting the temperature dependence of these limits," *Journal of loss prevention in the process industries*, vol. 25, no. 3, pp. 555–560, May 2012. [Online]. Available: https://www.ncbi.nlm.nih.gov/pmc/articles/PMC4676578/

[35] H. Le, Y. Liu, and M. S. Mannan, "Lower Flammability Limits of Hydrogen and Light Hydrocarbons at Subatmospheric Pressures," *Industrial & Engineering Chemistry Research*, vol. 52, no. 3, pp. 1372–1378, Jan. 2013. [Online]. Available: https://doi.org/10.1021/ie302504h

[36] T. Ma, "A thermal theory for estimating the flammability limits of a mixture," *Fire Safety Journal*, vol. 46, no. 8, pp. 558–567, Nov. 2011. [Online]. Available: http://www.sciencedirect.com/science/article/pii/S0379711211001263

[37] O. US EPA, "Review & Peer Review of "Parameters for Properly Designed and Operated Flares" Documents," Jun. 2016. [Online]. Available: https://www.epa.gov/stationary-sources-air-pollution/review-peer-review-parameters-properly-designed-and-operated-flares

[38] G. W. Jones, *Inflammability of mixed gases /*. Washington, D.C. :, 1929. [Online]. Available: http://hdl.handle.net/2027/mdp.39015078543314

[39] R. Bounaceur, P.-A. Glaude, B. Sirjean, R. Fournet, P. Montagne, M. Vierling, and M. Molière, "Prediction of Flammability Limits of Gas Mixtures Containing Inert Gases Under Variable Temperature and Pressure Conditions." American Society of Mechanical Engineers, Jun. 2017, pp. V04AT04A072–V04AT04A072. [Online]. Available: https://proceedings.asmedigitalcollection.asme.org/proceeding.aspx?articleid=2649966

[40] M. Terpstra, "Flammability limits of hydrogen-diluent mixtures in air," Thesis, University of Calgary, Aug. 2012. [Online]. Available: https://prism.ucalgary.ca/handle/11023/164

[41] "ASTM E681 - 09(2015) Standard Test Method for Concentration Limits of Flammability of Chemicals (Vapors and Gases)." [Online]. Available: https://www.astm.org/Standards/E681.htm

[42] "An improved test method for refrigerant flammability limits in a 12 L vessel: Science and Technology for the Built Environment: Vol 24, No 8." [Online]. Available: https://www.tandfonline.com/doi/abs/10.1080/23744731.2018.1434381?journalCode=uhvc21

[43] H. Wang, "Combustion Chemistry," Jun. 2015. [Online]. Available: https://cefrc.princeton.edu/sites/cefrc/files/Files/2015%20Lecture%20Notes/Wang/Lecture-7-Laminar-Premixed-Flames.pdf

[44] M. Huth and A. Heilos, *Modern Gas Turbine Systems*. Woodhead Publishing, 2013. [Online]. Available: https://www.sciencedirect.com/topics/chemistry/laminar-flame

[45] S. R. Turns *et al.*, *An introduction to combustion*. McGraw-Hill New York, 1996, vol. 499.

[46] P. Dirrenberger, H. Le Gall, R. Bounaceur, O. Herbinet, P.-A. Glaude, A. Konnov, and F. Battin-Leclerc, "Measurements of Laminar Flame Velocity for Components of Natural Gas," *Energy and Fuels*, vol. 25, no. 9, pp. 3875–3884, 2011. [Online]. Available: https://hal.archives-ouvertes.fr/hal-00776646

[47] M. C. Krejci, O. Mathieu, A. J. Vissotski, S. Ravi, T. G. Sikes, E. L. Petersen, A. Kérmonès, W. Metcalfe, and H. J. Curran, "Laminar Flame Speed and Ignition Delay Time Data for the Kinetic Modeling of Hydrogen and Syngas Fuel Blends," *Journal of Engineering for Gas Turbines and Power*, vol. 135, no. 2, pp. 021 503–021 503–9, Jan. 2013. [Online]. Available: http://dx.doi.org/10.1115/1.4007737

[48] Z. Chen, "On the accuracy of laminar flame speeds measured from outwardly propagating spherical flames: Methane/air at normal temperature and pressure," *Combustion and Flame*, vol. 162, no. 6, pp. 2442–2453, Jun. 2015. [Online]. Available: https://linkinghub.elsevier.com/retrieve/pii/S0010218015000541

[49] J. Johnplass, M. Henriksen, K. Vaagsaether, J. Lundberg, and D. Bjerketvedt, "Simulation of burning velocities in gases vented from thermal run-a-way lithium ion batteries," *Linköping University Electronic Press*, no. 138, pp. 157–161, Sep. 2017.

[50] T. Hirasawa, C. Sung, A. Joshi, Z. Yang, H. Wang, and C. Law, "Determination of laminar flame speeds using digital particle image velocimetry: Binary Fuel blends of ethylene, n-Butane, and toluene," *Proceedings of Combustion Institute*, vol. 29, no. 2, pp. 1427–1434, 2002.

[51] A. Kelley, A. Smallbone, D. Zhu, and C. Law, "Laminar flame speeds of C5 to C8n-alkanes at elevated pressures: Experimental determination, fuel similarity, and stretch sensitivity," *Proceedings of Combustion Institute*, vol. 33, no. 1, pp. 963–970, 2011.

[52] S. R. Mulpuru and G. B. Wilkin, "A model for vented deflagration of hydrogen in a volume," Atomic Energy of Canada Ltd., Tech. Rep. AECL–6826, 1982. [Online]. Available: http://inis.iaea.org/Search/search.aspx?orig_q=RN:13705575

[53] O. J. Ugarte, V. Akkerman, and A. S. Rangwala, "A computational platform for gas explosion venting," *Process Safety and Environmental Protection*, vol. 99, pp. 167–174, Jan. 2016. [Online]. Available: http://www.sciencedirect.com/science/article/pii/S0957582015001998

[54] H. Sezer, F. Kronz, V. Akkerman, and A. S. Rangwala, "Methane-induced explosions in vented enclosures," *Journal of Loss Prevention in the Process Industries*, vol. 48, pp. 199–206, Jul. 2017. [Online]. Available: http://www.sciencedirect.com/science/article/pii/S0950423017303601

[55] R. K. Kumar, H. TAMM, and W. C. HARRISON, "Combustion of Hydrogen at High Concentrations. Including the Effect of Obstacles," *Combustion Science and Technology*, vol. 35, pp. 175–186, 1983. [Online]. Available: http://www.tandfonline.com/doi/abs/10.1080/00102208308923709

[56] "NFPA 68: Standard on Explosion Protection by Deflagration Venting." [Online]. Available: https://www.nfpa.org/codes-and-standards/all-codes-and-standards/list-of-codes-and-standards/detail?code=68

[57] M. Vidal, W. Wong, W. J. Rogers, and M. S. Mannan, "Evaluation of lower flammability limits of fuel–air–diluent mixtures using calculated adiabatic flame temperatures," *Journal of Hazardous Materials*, vol. 130, no. 1, pp. 21–27, Mar. 2006. [Online]. Available: http://www.sciencedirect.com/science/article/pii/S0304389405004218

[58] F. Zhao, "_USInert Gas Dilution Effect on the Flammability Limits of Hydrocarbon Mixtures," Thesis, Feb. 2012. [Online]. Available: https://oaktrust.library.tamu.edu/handle/1969.1/ETD-TAMU-2011-12-10569

[59] F. Wu and G. Yushin, "Conversion cathodes for rechargeable lithium and lithium-ion batteries," *Energy & Environmental Science*, vol. 10, no. 2, pp. 435–459, Feb. 2017. [Online]. Available: http://pubs.rsc.org/en/content/articlelanding/2017/ee/c6ee02326f